Evaluation of fiber Bragg grating sensor interrogation using InGaAs linear detector arrays and Gaussian approximation on embedded hardware

Saurabh Kumar,[1,2] Bharadwaj Amrutur,[3,4] and Sundarrajan Asokan[1]
[1]*Department of Instrumentation and Applied Physics, Indian Institute of Science, Bangalore 560012, India*
[2]*Research and Technology Centre–India, Robert Bosch Engineering and Business Solutions Pvt. Ltd., 560095 Bangalore, India*
[3]*Department of Electrical Communication Engineering, Indian Institute of Science, Bangalore 560012, India*
[4]*Robert Bosch Centre for Cyber Physical Systems, Indian Institute of Science, Bangalore 560012, India*

(Received 6 April 2017; accepted 15 January 2018; published online 2 February 2018)

Fiber Bragg Grating (FBG) sensors have become popular for applications related to structural health monitoring, biomedical engineering, and robotics. However, for successful large scale adoption, FBG interrogation systems are as important as sensor characteristics. Apart from accuracy, the required number of FBG sensors per fiber and the distance between the device in which the sensors are used and the interrogation system also influence the selection of the interrogation technique. For several measurement devices developed for applications in biomedical engineering and robotics, only a few sensors per fiber are required and the device is close to the interrogation system. For these applications, interrogation systems based on InGaAs linear detector arrays provide a good choice. However, their resolution is dependent on the algorithms used for curve fitting. In this work, a detailed analysis of the choice of algorithm using the Gaussian approximation for the FBG spectrum and the number of pixels used for curve fitting on the errors is provided. The points where the maximum errors occur have been identified. All comparisons for wavelength shift detection have been made against another interrogation system based on the tunable swept laser. It has been shown that maximum errors occur when the wavelength shift is such that one new pixel is included for curve fitting. It has also been shown that an algorithm with lower computation cost compared to the more popular methods using iterative non-linear least squares estimation can be used without leading to the loss of accuracy. The algorithm has been implemented on embedded hardware, and a speed-up of approximately six times has been observed. *Published by AIP Publishing.* https://doi.org/10.1063/1.5022548

I. INTRODUCTION

Usage of Fiber Bragg Grating (FBG) sensors has gained prominence in structural health monitoring[1] and biomedical applications.[2] Their small size and the possibility of using them in MRI environments have enabled their usage in needles for medical procedures.[3–6] Their high sensitivity has enabled their usage as force sensors in smart surgical instruments for technically demanding applications like retinal microsurgery.[7] Having multiple sensors in an arrayed form has enabled their usage in both structural health monitoring of large structures like bridges[8] and sensors for closed loop control of robotic devices.[9]

A fiber Bragg grating consists of periodic modulation of the refractive index in the core of an optical fiber. Light is scattered by each grating plane and on satisfaction of the Bragg condition, constructively adds up to form a back reflected peak as shown in Fig. 1(a). A sample FBG spectrum obtained using an optical spectrum analyzer is shown in Fig. 1(b). The center wavelength of the back reflected signal (λ_b) is a function of grating pitch (Λ) and the effective refractive index of the fiber core (n_{eff}) as given by the following equation:

$$\lambda_b = 2\Lambda n_{eff}, \tag{1}$$

The successful and widespread adoption of FBG sensors for biomedical applications is dependent not only on sensor characteristics but also on FBG interrogation systems. The interrogation system provides a means to measure the wavelength shift. One of the earliest FBG interrogation methods proposed, which has also been modified and adapted over the years, consists of using an edge filter providing a linear relationship between wavelength shifts and output intensity change.[10–13] Though it is effective, scaling it to multiple sensors is difficult. Another alternative method has been based on matched FBGs.[14–16] Though good accuracy can be achieved, the constraint of using closely matched FBGs in both sensing and measurement arms in this method poses challenges in usage. Another method for which several extensions have been proposed over the years is based on the use of tunable Fabry–Pérot filter[17,18] whose passband is locked to the back reflected signal of the FBG using a feedback loop. This method provides high accuracy, but using piezo-actuation to tune the Fabry–Pérot filter constrains the interrogation rate.

In recent years, methods based on the use of wavelength tunable sources have been popular. Different configurations have been exploited including wavelength swept fiber lasers with the Fabry–Pérot filter in the cavity to sweep the laser output wavelength,[19] wavelength swept fiber lasers with intracavity acousto-optic tunable filter,[20] swept fiber laser based on dispersion tuning technique which does not require any optical tunable filter in the laser cavity,[21] Fourier domain mode

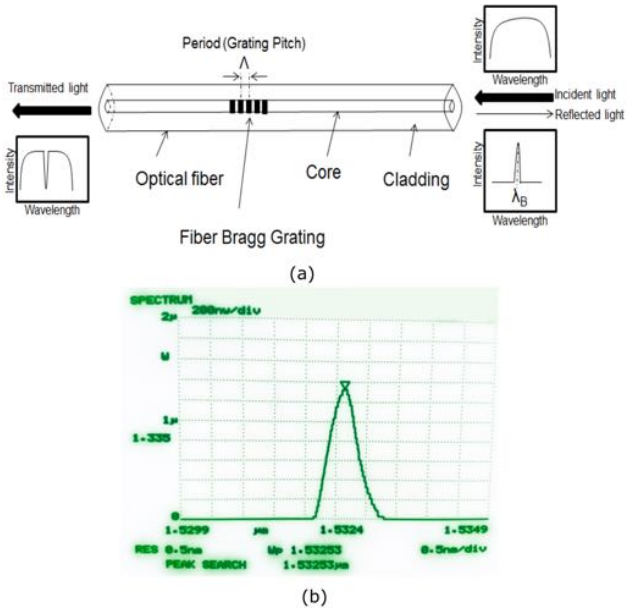

FIG. 1. (a) Schematic diagram showing reflected peak for a fiber Bragg grating and (b) spectrum obtained for the back reflected peak using an optical spectrum analyzer.

locking laser,[22,23] and active mode locking laser.[24] Interrogation systems based on tunable swept laser based systems can provide high resolution and dynamic range. They also enable interrogation of a large number of sensors per fiber over very large distances.

Another method which has gained popularity in recent years is based on the use of a diffraction grating as a dispersion element in combination with linear detector arrays. Low power broadband sources and low reflectivity gratings can be used with this method. For several biomedical and robotic applications, where the number of sensors per fiber and the distance between the sensors and light source are small, this can be a useful option. It is required to meet the application specific requirements for accuracy and resolution along with required sampling rates and feasibility of creating systems with integrated embedded hardware for real-time computations.

The main components of such a system are the diffraction grating which acts as a dispersion element and a linear detector array along with the readout electronics. Both transmission and reflection gratings can be used in different configurations. For interrogation in the near-infrared region, InGaAs linear detector arrays can be used. Figure 2 shows the schematic diagram of an interrogation system based on the transmission grating and InGaAs linear detector array. Commercially available linear image sensors package the InGaAs linear detector array with the charge amplifier array, offset compensation circuit, shift register, and timing generator.

The main challenge in using these interrogation systems is achieving the required resolution. For example, an InGaAs linear photodiode array with 512 pixels with a wavelength range of 1510 nm–1595 nm provides an Full Width at Half Maximum (FWHM) resolution of approximately 330 pm. This is not sufficient for most applications, but curve-fitting methods[25,26] have been used to achieve sub-pixel accuracy. However, the effect of the choice of number of pixels from a spectrum peak

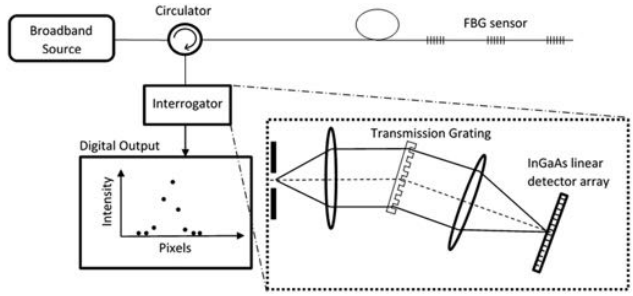

FIG. 2. Schematic diagram of an FBG interrogation system based on the transmission grating and an InGaAs linear detector array (based on Ibsen Photonics' Spectrometer design guide http://ibsen.com/technology/spectrometer-design-guide/).

and the choice of algorithms has a significant impact on the accuracy. In this work, a detailed analysis of the effect of the choice of number of pixels on the accuracy of the estimated Bragg wavelength and the points where errors are highest is provided. This is important because specifications related to minimum errors are not sufficient for determining usage in several applications. It is useful to decide the use of algorithms based on the knowledge of average and maximum errors and the conditions which result in maximum errors. Also, it is useful to implement the algorithm on embedded hardware, and hence it is important to consider computational complexity to meet the sampling rate requirements.

II. MEASUREMENT SETUP AND DATA CHARACTERISTICS

Two commercially available interrogation systems—I-MON 512 USB from Ibsen Photonics and SM130 from Micron Optics—have been used for this work. SM130 is based on a swept tunable laser, while the I-MON 512 USB uses a transmission grating along with an InGaAs linear detector array with 512 pixels (Hamamatsu G11620-512DA). I-MON 512 has been selected because it allows direct access to the measured intensity at each pixel and the choice of algorithm for peak estimation is left to the user. The focus of this work is on the comparison of algorithms and they would be applicable for any similar system.

A. Setup

Most sensing applications using FBG sensors are based on measuring the wavelength shift in response to strain or temperature changes. Hence, for the analysis of the algorithms, six FBG sensors have been fabricated on a single germanosilicate fiber using the phase mask technique and small incremental strains have been applied using the setup as shown in Fig. 3. The sensors have been fabricated using three different phase masks. For each phase mask, two sensors have been fabricated close to each other with a separation of approximately 15 mm by pre-stretching the fiber and translating it. The wavelength separation between these two sensors is approximately 1.5 nm.

The fiber has been fixed rigidly to both the translation stage and the fixed end. Not having the fiber bonded to another material avoids any non-linearity or spectrum distortion

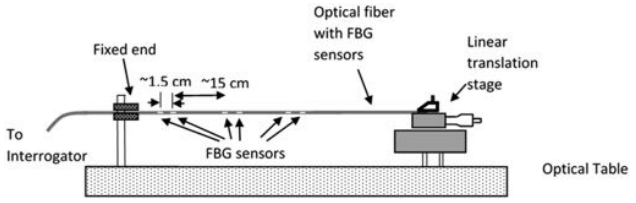

FIG. 3. Setup to generate data samples.

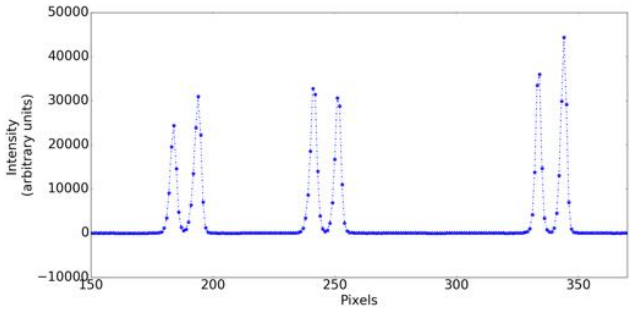

FIG. 4. Spectrum obtained from the linear detector array.

arising because of the bonding. Since the strain on each sensor has been applied through elongation by using the translation stage, and measurements for each sensor have been made simultaneously, the effect of slight variations in ambient temperature can be neglected as the temperature variation for all sensors is similar.

B. Data characteristics

The translation stage has been linearly moved for 10 steps. At each step, the data have been acquired using both the interrogation systems and have been logged in files. The log of data from I-MON 512 consists of the measured intensity at each pixel of the 512 pixel array. The log of data from SM130 consists of the peak wavelength corresponding to each sensor.

There are small variations in the applied strain at each measurement step because of small inaccuracies in the linear translation stage. However, the variation is not relevant for this evaluation as error comparisons have been made for each measurement point. Figure 4 shows the spectrum obtained from the linear detector array for one sample measurement. A linear interpolation has been added between the points to make visualization of peaks easier.

III. BRAGG WAVELENGTH ESTIMATION

The linear detector array only provides the intensity at each pixel. Using the pixel with highest intensity as the one representing peak wavelength would lead to very low resolution. Hence the peak wavelength has to be estimated using an approximation algorithm providing sub-pixel resolution.

A. Centroid algorithm

The simplest method to achieve sub-pixel resolution is based on the centroid[27] algorithm as shown in the following equation:

$$\lambda_b = \frac{\sum_{i=1}^{N} \lambda_i I_i}{\sum_{i=1}^{N} \lambda_i}, \tag{2}$$

where λ_i are the wavelengths at the pixels around the peak and I_i are the corresponding intensity values.

The algorithm has been applied to estimate wavelength shifts for all sensors for all the measurements corresponding to incremental strains. The values along with that measured using the swept tunable laser based interrogation system is shown in Fig. 5. As can be seen, the deviation is as high as 102 pm for some points when using 3 pixels and 70 pm when using 5 pixels.

The spectrum shift at the points where the deviation is maximum has been analyzed. It has been found that the deviation is maximum when the spectrum shifts to include a new pixel. This can be seen in the comparison as shown in Fig. 6. For the wavelength shift due to strain difference between measurement 0 and measurement 1, the spectrum for sensor 1 shifts across pixels. This does not happen for the other sensors. Similarly, for the wavelength shift between measurement 2 and measurement 3, the spectrum shifts across pixels for sensor 6. The errors in estimation are highest at these points as also seen in Fig. 5. Such high errors make this method unsuitable for use when small wavelength shifts have to be detected.

B. Gaussian approximation for the FBG spectrum and least squares estimation of Bragg wavelength

The FBG spectrum can be approximated as a Gaussian[28] as represented by the following equation:

$$I(\lambda, A, \lambda_b, \sigma) = Ae^{-\frac{(\lambda-\lambda_b)^2}{2\sigma^2}}, \tag{3}$$

where λ_b represents the Bragg wavelength.

Given the wavelengths at the pixels (λ_i) and the intensities (I_i), from the measurements, the goal is to estimate the parameters λ_b, A, and σ. This can be done using least squares estimation. The error function can be represented as shown in the following equation:

$$E = \sum_{i=1}^{N} (I(\lambda_i, A, \lambda_b, \sigma) - I_i)^2. \tag{4}$$

This has to be minimized with respect to the parameters λ_b, A, and σ. Though there are several methods that can be used to solve this, the Levenberg-Marquard algorithm[29] has been extensively used and is the default implementation in most libraries (e.g., the least squares curve fitting function in LabView uses it). In this evaluation, the implementation in the SciPy[30] library in Python which internally uses the MINPACK implementation[31] has been used.

To apply the non-linear least squares estimation, it is first required to find the pixels in the neighborhood of peaks. For extracting these pixels from the data for all the 512 pixels in the spectrum, a simple peak search algorithm has been employed. This first applies a threshold based on the intensity of the highest intensity peak in the spectrum to get all possible peak regions. Then the change in gradient of the difference in intensities has been used to detect all the pixels with highest

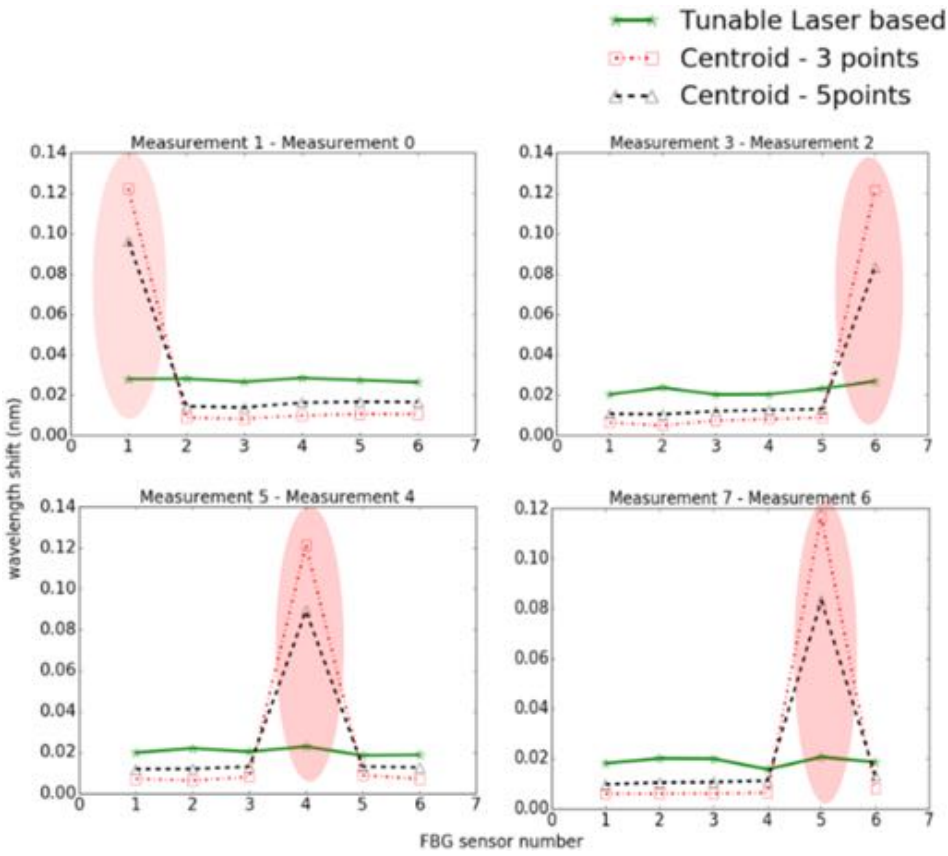

FIG. 5. Errors in peak wavelength estimation using the centroid method compared to using an interrogation system based on the swept tunable laser for one particular sensor across different measurements.

intensities in a neighborhood. This method enables handling of sensors with varying reflectivity. The need for this is evident by observing the spectrum in Fig. 4 where the smallest peak has an intensity approximately 50% of that of the highest peak. Once all the pixels with highest intensities have been obtained, the least squares method can be employed based on different number of pixels around the pixel with maximum intensity.

The Levenberg-Marquardt algorithm requires setting of initial values for the parameters which are being estimated. The wavelength of the pixel with highest intensity and the intensity at that pixel have been used as the initial values for λ_b and A, respectively.

To evaluate the variations in the estimated peak wavelength, the last square estimation has been performed using four different sets of pixels. In the following discussion, the peak refers to the pixel with highest intensity. The first variation uses one pixel to the left and one to the right of peak, the second uses four pixels with two pixels to the left of the peak, the third uses four pixels with two pixels to the right of the peak, and the fourth uses five pixels with two pixels on both sides of the peak. Figure 7 shows the estimated wavelengths for all sensors for all measurements. The measurements where high deviation is observed have been highlighted.

Since accuracy in the measurement of wavelength shift is important, it is analyzed for all sensors for each measurement

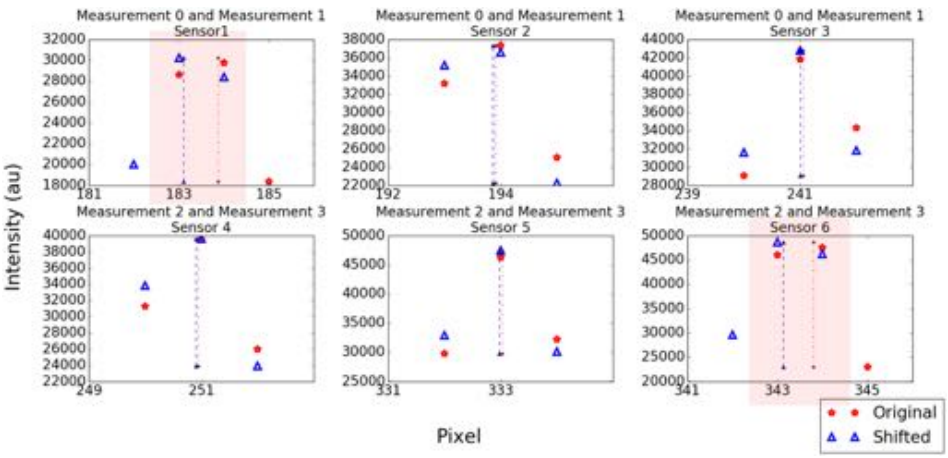

FIG. 6. Plots showing the points around the peak. Each measurement corresponds to a shift in wavelength due to applied strain. The original and the shifted points and the estimated peak using the centroid algorithm are shown for three different sensors on the fiber. The measurements corresponding to maximum errors have been highlighted.

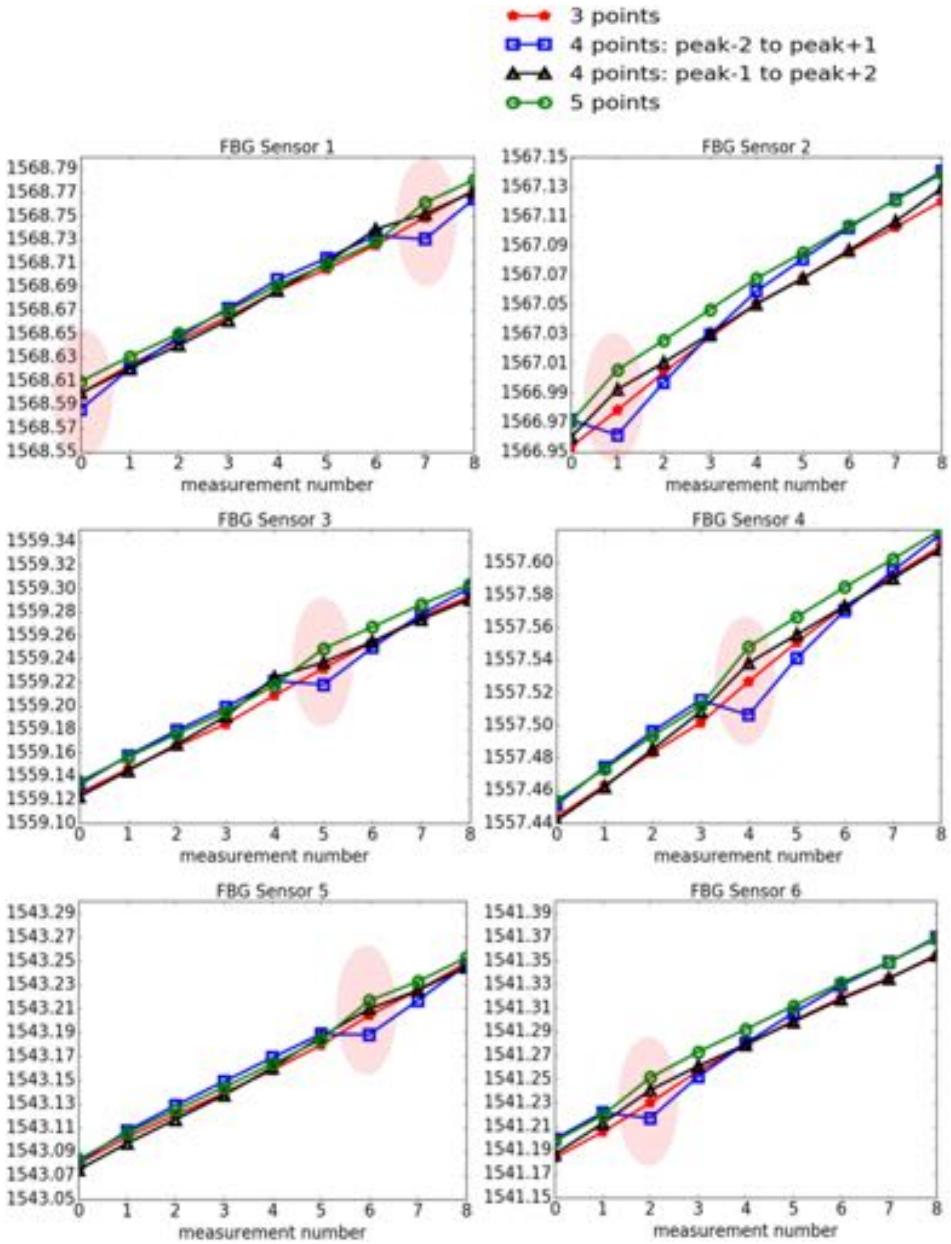

FIG. 7. Estimated Bragg wavelengths using different number of pixels around the peak. The points where the maximum difference in estimated wavelengths occurs have been highlighted.

point. The comparisons have also been made to the wavelength shift measured by the interrogator based on the swept tunable laser. It has been found that the accuracy varies with the different number of pixels used in the non-linear least squares estimation as can be seen in Fig. 8 for two sample wavelength shift measurements.

To find the main source of high variation at certain points, the spectrum shift at these points has been analyzed. It has been found that similar to the centroid algorithm, the maximum variation occurs when the spectrum shifts completely one pixel to the left or right. This is seen in Fig. 9. For the purpose of curve fitting, pixels are assumed as points (representing the center of the pixel) and the intensities as the values at these points. In reality, the intensity is spread across the pixels. Hence, when the spectrum shift corresponding to the wavelength shift from one measurement to the next is not limited to the same set of pixels, the error is higher. Unlike in the case of centroid algorithm, using five pixels instead of three does not improve the accuracy. It actually reduces it as the curve fitting works best only when the pixels are within the Full Width at Half Maximum (FWHM) range. Since all measurements were done by applying increasing strain, the wavelength shift is in the same direction. This is the direction toward the left in terms of pixels in the linear detector array as the pixel number one represents the maximum wavelength limit of 1595 nm. Hence, at the error points, the impact is highest on the peak estimation using four points where the two points are to the left of the pixel with highest intensity as there is a high asymmetry around the peak after the shift.

Figure 9 clearly shows that a new set of pixels are used for the Bragg wavelength estimation for sensor 1 after the shift in wavelength while the same set of pixels are used before and after the wavelength shift for sensor 2. The effect of errors in wavelength shift estimation can be most

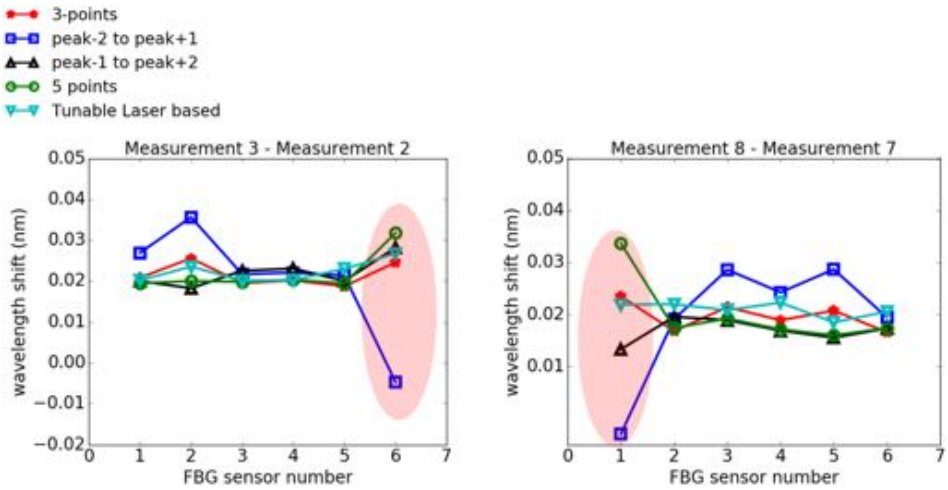

FIG. 8. Wavelength shift estimation using different number of pixels for sample measurements. The points where maximum differences are observed compared to a tunable laser based system have been highlighted.

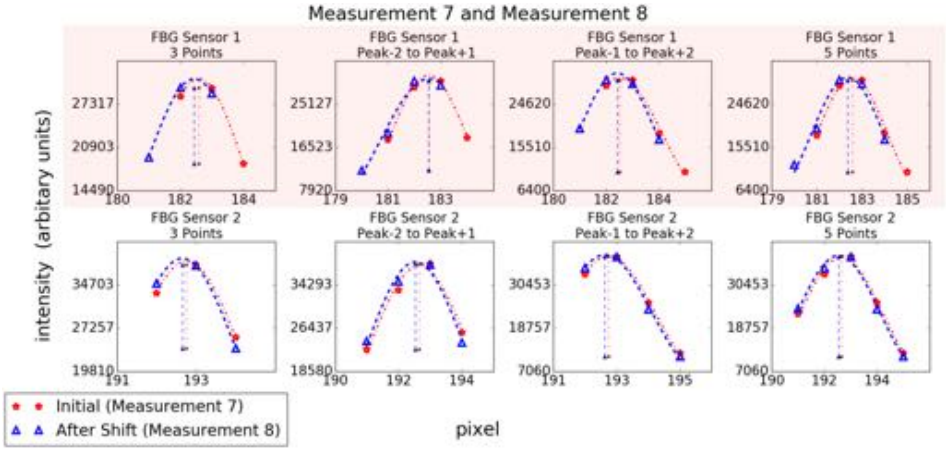

FIG. 9. Spectrum for sensor 1 and sensor 2 for two consecutive measurements. In the case of sensor one, a new set of pixels are used for estimation after the wavelength shift, while in the case of sensor 2 the same set of pixels are used before and after the wavelength shift.

prominently seen in the first row of images corresponding to sensor 1 when 4 pixels have been used in the estimation. This leads to the high differences in wavelength shift estimation as compared to the tunable laser based interrogation system as seen in the corresponding plot in Fig. 8. Figure 10 shows the difference between the estimated wavelength shifts using the Gaussian approximation with different number of pixels and that measured using the swept tunable laser based interrogation system for all six sensors for eight wavelength shift measurements. The advantage of using three pixels can be clearly seen.

The results have been summarized in Table I. Even though the median difference between the estimated values and those measured using tunable laser based systems are less than 1 pm, the maximum errors are much higher when using 4 points and 5 points as compared to 3 points. This is attributed to the measurements when the spectrum shifts across the pixels.

Comparison of errors using curve fitting with the Levenberg-Marquardt method and using the centroid algorithm highlights the specific advantage of using the Levenberg-Marquardt method specifically to reduce the maximum errors.

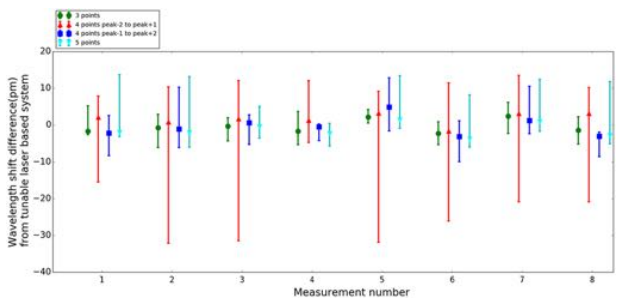

FIG. 10. Differences in wavelength shift estimation using least squares methods for the Gaussian approximation and measurement using the swept tunable laser based interrogation system.

TABLE I. Wavelength shift difference from the tunable laser based system using different number of points for non-linear least squares estimation using the Levenberg-Marquardt algorithm.

	3 points	4 points (peak −2 to peak +1)	4 points (peak −1 to peak +2)	5 points
Maximum wavelength shift difference (pm)	6	32	12	14
Median wavelength shift difference (pm)	0.3	1.7	0.8	0.8

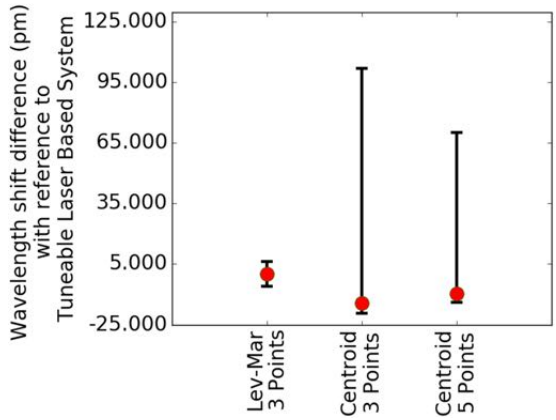

FIG. 11. Comparison of errors in wavelength shift measurement relative to the tunable laser based interrogation system.

This can be seen in Fig. 11. The maximum error using the centroid fit can be up to 102 pm using 3 points and 70 pm using 5 points while that with the Levenberg-Marquardt method and 3 points is limited to 6 pm. The median error is also significantly reduced from close to 15 pm for centroid with 3 points to less than 1 pm for Levenberg-Marquardt with 3 points as summarized in Table II.

C. Lower computational cost algorithm utilizing Gaussian approximation for the FBG spectrum

In Sec. III B, it has been shown that Bragg wavelength estimation using the non-linear least squares estimation and Gaussian approximation for interrogation systems based on InGaAs linear detector arrays can achieve accuracy very close to those achieved by interrogation systems based on the swept tunable laser. The errors are lowest when using three pixels for the least squares estimation such that the center pixel is the one with the highest intensity. However, the computational cost of non-linear least squares estimation is high in spite of using the Levenberg-Marquardt algorithm. To overcome this, Caruana's algorithm[32,33] has been evaluated which is specific to curve fitting for the Gaussian function and does not require any iterative method. Caruana's algorithm reduces the estimation to solving simultaneous linear equations which can be done efficiently using matrix manipulation methods.

TABLE II. Wavelength shift difference from the tunable laser based system using the Levenberg-Marquardt algorithm and Centroid Algorithm.

	Levenberg-Marquardt 3 points	Centroid 3 points	Centroid 5 points
Maximum wavelength shift difference (pm)	6	102	70
Median wavelength shift difference (pm)	0.3	14.4	9.6

Taking natural logarithm on both sides for Eq. (3),

$$\ln I = \ln A - \frac{(\lambda - \lambda_b)^2}{2\sigma^2}, \tag{5}$$

$$= \ln A - \frac{\lambda^2}{2\sigma^2} + \frac{2\lambda_b\lambda}{2\sigma^2} - \frac{{\lambda_b}^2}{2\sigma^2}, \tag{6}$$

$$= a + b\lambda + c\lambda^2, \tag{7}$$

where $a = \ln A - \frac{{\lambda_b}^2}{2\sigma^2}$, $b = \frac{\lambda_b}{\sigma^2}$, $c = -\frac{1}{2\sigma^2}$.

For measured intensities I_i at pixels with wavelengths λ_i, this is equivalent to fitting a parabola to the points. Formulating it as a least squares estimation problem, the error term to be minimized can be written as

$$E = \sum_{i=1}^{N} \left(\ln I_i - a - b\lambda_i - c{\lambda_i}^2\right)^2. \tag{8}$$

Minimization can be done by solving

$$\frac{\partial E}{\partial a} = 0, \tag{9}$$

$$\frac{\partial E}{\partial b} = 0, \tag{10}$$

$$\frac{\partial E}{\partial c} = 0. \tag{11}$$

Solving (9)–(11), respectively,

$$\sum_{i=1}^{N} \ln I_i - aN - b\sum_{i=1}^{N} \lambda_i - c\sum_{i=1}^{N} {\lambda_i}^2 = 0, \tag{12}$$

$$\sum_{i=1}^{N} \lambda_i \ln I_i - a\sum_{i=1}^{N} \lambda_i - b\sum_{i=1}^{N} {\lambda_i}^2 - c\sum_{i=1}^{N} {\lambda_i}^3 = 0, \tag{13}$$

$$\sum_{i=1}^{N} {\lambda_i}^2 \ln I_i - a\sum_{i=1}^{N} {\lambda_i}^2 - b\sum_{i=1}^{N} {\lambda_i}^3 - c\sum_{i=1}^{N} {\lambda_i}^4 = 0, \tag{14}$$

$$\begin{bmatrix} N & \sum_{i=1}^{N}\lambda_i & \sum_{i=1}^{N}{\lambda_i}^2 \\ \sum_{i=1}^{N}\lambda_i & \sum_{i=1}^{N}{\lambda_i}^2 & \sum_{i=1}^{N}{\lambda_i}^3 \\ \sum_{i=1}^{N}{\lambda_i}^2 & \sum_{i=1}^{N}{\lambda_i}^3 & \sum_{i=1}^{N}{\lambda_i}^4 \end{bmatrix} \begin{bmatrix} a \\ b \\ c \end{bmatrix} = \begin{bmatrix} \sum_{i=1}^{N}\ln I_i \\ \sum_{i=1}^{N}\lambda_i \ln I_i \\ \sum_{i=1}^{N}{\lambda_i}^2 \ln I_i \end{bmatrix}, \tag{15}$$

$$\lambda_b = -\frac{b}{2c}. \tag{16}$$

This is in the standard form $\boldsymbol{A}\mathbf{x} = \mathbf{b}$. The terms with higher powers in $\boldsymbol{A}$ can be computed efficiently by using vector representations for data points and dot products. Since, for the purpose of this evaluation, all implementations have been done in Python, these can be very efficiently done. In order to estimate the gain in efficiency, the Bragg wavelength estimation has been done both with the non-linear least squares estimation using the Levenberg-Marquardt algorithm and Caruana's algorithm in comparison to the centroid algorithm. The execution time has been measured on a Raspberry Pi 2 model B board with a 900 MHz quad core ARM Cortex—A7 central processing unit (CPU) and 1 GB of RAM and running the Rasbian operating system which is based on the Debian operating system. The method for timing estimate has been done using the standard recommended method in Python using the *timeit* library.

TABLE III. Comparison of execution times and difference in estimated wavelength from the tunable laser based system for the three methods.

	Centroid 3 points	Levenberg-Marquardt 3 points	Caruana 3 points
Median normalized execution time	1×	64×	10×
Maximum wavelength shift difference from the tunable laser based system (pm)	100	6	6
Median wavelength shift difference from the tunable laser based system (pm)	15	0.3	0.3

The results have been summarized in Table III. As can be seen, the execution time is significantly lower for Caruana's algorithm as compared to the Levenberg-Marquardt algorithm. It has been observed that using Caruana's algorithm provides an average speed-up of approximately 6.5 times. Using the Levenberg Marquard algorithm with the used setup reduces the maximum sampling frequency to around 30 Hz. However, using Caruana's algorithm allows a sampling rate around 200 Hz. The estimated values for the Bragg wavelength have also been compared. The difference between Caruana's algorithm and Levenberg-Marquardt is less than 0.01 pm which is sufficient to recommend the use of Caruana's algorithm over non-linear least squares estimation using the Levenberg-Marquardt algorithm with three pixels on embedded hardware.

There is another advantage of using Caruana's algorithm. When the strain changes slowly compared to the sampling rate and the pixels for each peak do not change, there is no need to recalculate the matrix $\boldsymbol{A}$. This would further reduce the required computation for each sample. However, this was not used in the computation time evaluation here to avoid any dependency on specific data.

IV. CONCLUSION AND FUTURE WORK

This evaluation has shown that FBG interrogation systems based on InGaAs linear detector arrays combined with curve fitting methods utilizing the Gaussian approximation of the FBG spectrum can achieve accuracy close to that achieved by interrogation systems based on the swept tunable laser. This can be useful for biomedical and robotic applications where the number of sensors and distance between the sensors and the interrogation system are small, and benefits other than high resolution of a swept laser baser system are not utilized. It has been shown that the choice of number of pixels around the peak has a significant impact on the maximum errors when using the non-linear least squares estimation based on the Levenberg-Marquardt algorithm. It has also been shown that Caruana's algorithm provides the same accuracy as the Levenberg-Marquardt algorithm while being significantly computationally faster. This has been demonstrated through implementation on an embedded hardware platform which can be packaged with the linear detector array and the transmission gratings. In future, it is intended to demonstrate the suitability for an application like estimation of forces during robotic needle insertion into tissues.

ACKNOWLEDGMENTS

We acknowledge the funding for this work from Robert Bosch Centre for Cyber Physical Systems at Indian Institute of Science, Bangalore.

[1]H. N. Li, D. S. Li, and G. B. Song, Eng. Struct. **26**(11), 1647–1657 (2004).
[2]S. Umesh and S. Asokan, J. Indian Inst. Sci. **94**(3), 319–328 (2014).
[3]Y. L. Park *et al.*, IEEE/ASME Trans. Mechatronics **15**(6), 906–915 (2010).
[4]R. J. Roesthius, M. Kemp, J. J. van den Dobbelsteen, and S. Misra, IEEE/ASME Trans. Mechatronics **19**(4), 1115–1126 (2014).
[5]K. R. Henken, J. Dankelman, J. J. Dobbelsteen, L. K. Cheng, and M. S. Heiden, IEEE/ASME Trans. Mechatronics **19**(5), 1523–1531 (2014).
[6]S. Kumar, V. Shrikanth, B. Amrutur, S. Asokan, and M. S. Bobji, J. Biomed. Opt. **21**(12), 127009 (2016).
[7]X. He, J. Handa, P. Gehlbach, R. Taylor, and I. Iordachita, IEEE Trans. Biomed. Eng. **61**(2), 522–534 (2014).
[8]J. M. Ko and Y. Q. Ni, Eng. Struct. **27**(12), 1715–1725 (2005).
[9]H. Song, K. Kim, and J. Lee, Rev. Sci. Instrum. **82**(7), 074301 (2011).
[10]S. M. Melle, K. Liu, and R. M. Measures, IEEE IEEE Photonics Technol. Lett. **4**, 516–518 (1992).
[11]T. Guo, H.-Y. Tam, and J. Albert, in CLEO: Science and Innovations, 2011.
[12]U. Tiwari, K. Thyagarajan, M. R. Shenoy, and S. C. Jain, IEEE Sens. J. **13**, 1315–1319 (2013).
[13]N. Stan, D. C. Bailey, S. L. Chadderdon, S. Webb, M. Zikry, K. J. Peters, R. H. Selfridge, and S. M. Schultz, Meas. Sci. Technol. **25**, 065206 (2014).
[14]D. A. Jackson, L. Reekie, J. L. Archambault, and A. B. L. Ribeiro, Opt. Lett. **18**, 1192–1194 (1993).
[15]M. A. Davis and A. D. Kersey, Electron. Lett. **31**, 822–823 (1995).
[16]J. Cui, Y. Hu, K. Feng, J. Li, and J. Tan, Sensors **15**, 16516–16535 (2015).
[17]A. D. Kersey, T. A. Berkoff, and W. W. Morey, Opt. Lett. **18**, 1370–1372 (1993).
[18]W. R. Allan, Z. W. Graham, J. R. Zayas, D. P. Roach, and D. A. Horsley, IEEE Sens. J. **9**, 936–943 (2009).
[19]S. H. Yun, D. J. Richardson, and B. Y. Kim, Opt. Lett. **23**, 843–845 (1998).
[20]S. H. Yun, D. J. Richardson, D. O. Culverhouse, and B. Y. Kim, IEEE J. Sel. Top. Quantum Electron. **3**, 1087–1096 (1997).
[21]Y. Nakazaki and S. Yamashita, Opt. Express **17**, 8310–8318 (2009).
[22]D. Chen, C. Shu, and S. He, Opt. Lett. **33**, 1395–1397 (2008).
[23]E. J. Jung, C.-S. Kim, M. Y. Jeong, M. K. Kim, M. Y. Jeon, W. Jung, and Z. Chen, Opt. Express **16**, 16552–16560 (2008).
[24]H. D. Lee, G. H. Kim, T. J. Eom, M. Y. Jeong, and C.-S. Kim, J. Lightwave Technol. **33**, 2617–2622 (2015).
[25]T. Bodendorfer, M. S. Muller, F. Hirth, and A. W. Koch, in *Proceedings of International Symposium on Optomechatronic Technologies* (IEEE, 2009), pp. 122–126.
[26]J. Jiang, T. Liu, K. Liu, and Y. Zhang, Opt. Eng. **51**(3), 034403–034411 (2012).
[27]A. Ezbiri, S. E. Kanellopoulos, and V. A. Handerek, Opt. Commun. **150**(1), 43–48 (1998).
[28]J. M. Gong *et al.*, IEEE Photonics Technol. Lett. **14**(5), 678–680 (2002).
[29]J. J. Moré, *Numerical Analysis* (Springer, Berlin, Heidelberg, 1978), pp. 105–116.
[30]T. E. Oliphant, "Python for scientific computing," Comput. Sci. Eng. **9**(3), 19–20 (2007).
[31]J. J. Moré, D. C. Sorensen, K. E. Hillstrom, and B. S. Garbow, *Sources and Development of Mathematical Software* (Prentice-Hall, 1984), pp. 88–111.
[32]R. A. Caruana, R. B. Searle, T. Heller, and S. I. Shupack, Anal. Chem. **58**(6), 1162–1167 (1986).
[33]H. Guo, IEEE Signal Process. Mag. **28**(5), 134–137 (2011).